Letter

Bypassing thermalization timescales in temperature estimation using prethermal probes

Nicholas Anto-Sztrikacs,[1,*] Harry J. D. Miller,[2] Ahsan Nazir,[2] and Dvira Segal[3,1,†]
[1]*Department of Physics, 60 Saint George Street, University of Toronto, Toronto, Ontario, Canada M5S 1A7*
[2]*Department of Physics and Astronomy, University of Manchester, Oxford Road, Manchester M13 9PL, United Kingdom*
[3]*Department of Chemistry and Centre for Quantum Information and Quantum Control, University of Toronto, 80 Saint George Street, Toronto, Ontario, Canada M5S 3H6*

(Received 10 November 2023; accepted 15 May 2024; published 27 June 2024)

We introduce prethermal temperature probes for sensitive, fast, and robust temperature estimation. While equilibrium thermal probes with a manifold of quasidegenerate excited states have been previously recognized for their maximal sensitivity, they suffer from long thermalization timescales. When considering *time* as a critical resource in thermometry, it becomes evident that these equilibrium probes fall short of ideal performance. Here, we propose a different paradigm for thermometry, where setups originally suggested for optimal *equilibrium* thermometry should instead be employed as *prethermal* probes, by making use of their long-lived quasiequilibrium state. This transient state emerges from the buildup of quantum coherences among quasidegenerate levels. For a class of physically motivated initial conditions, we find that energy measurements of the prethermal state exhibit a similar sensitivity as the equilibrium state. However, they offer the distinct benefit of orders of magnitude reduction in the time required for the estimation protocol. Upon introducing a figure of merit that accounts for the estimation protocol time, prethermal probes surpass the corresponding equilibrium probes in terms of effective thermal sensitivity, opening avenues for rapid thermometry by harnessing the long-lived prethermal states.

DOI: 10.1103/PhysRevA.109.L060201

Introduction. The classical notion of thermometry is rooted in the zeroth law of thermodynamics whereby the temperature of a sample is inferred using a small ancillary system, a probe. This probe is brought into contact with the sample until thermal equilibrium is reached [1,2]. Subsequently, the temperature of the sample is inferred by measuring a physically relevant observable of the probe [3,4]. From this protocol, it follows that an ideal probe should offer temperature estimates that are both *accurate* and *rapid*. These principles also apply in quantum thermometry, where a classical probe is now replaced by a quantum system. Focusing on precision, the figure of merit quantifying the sensitivity of a probe is captured by the quantum Fisher information, an information-theoretic tool that by the Cramér-Rao inequality upper bounds the signal-to-noise ratio of temperature estimates [1,5].

Equilibrium thermometry is a common approach to temperature sensing in the nanoscale regime [6–9]. In this method, the estimation protocol relies on the probe achieving a state of thermal equilibrium with the sample. These probes are straightforward to operate since energy measurements maximize their signal-to-noise ratio [10,11]. By maximizing the Fisher information of equilibrium probes it was proved that the most sensitive thermometers are effective two-level systems with a single ground state and N quasidegenerate excited levels [11,12]. Furthermore, the effects of anharmonic probes [13], and multiple probes, in both the noninteracting [10,14–16] and interacting [17–19] cases have been analyzed. However, equilibration times for probes with highly degenerate levels are substantial, and hence require a long time for (thermal) state preparation [20]. Though time is not a standard parameter in theoretical thermometry, in practice it plays a crucial role due to the resource nature of thermal state preparation time in quantum sensing [21,22]. To accelerate temperature estimation, *transient* temperature estimation schemes, either through pure decoherence processes [23–25] or where the probe does not fully thermalize with the sample [26–31] have been proposed. However, so far such attempts suffer from fundamental issues [32]. Notably, there is no generic measurement operator of the probe that optimizes the temperature estimate. Furthermore, the Fisher information can strongly fluctuate as the quantum state of the probe evolves, requiring operating transient probes in a highly controlled fashion.

Here, we propose a strategy for nanoscale temperature estimation. This approach leverages the accuracy and robustness of equilibrium thermometry with the flexibility and speed of transient thermometry, by putting forward a class of probes that are fast, accurate, robust, and physically motivated. We do this by introducing the concepts of *prethermal thermometry* and time-weighted (classical/quantum) Fisher information as the relevant figure of merit. Prethermal states materialize when there is a large separation of timescales in the equilibration dynamics [33–35]. In this case, before reaching the true equilibrium state, the system first approaches a *quasiequilibrium* state, which is long lived. As we demonstrate in this Letter, such prethermal states offer a robust platform for temperature measurements. We consider energy measurements in this work due to their simplicity and direct

*Contact author: nicholas.antosztrikacs@mail.utoronto.ca
†Contact author: dvira.segal@utoronto.ca

comparison with equilibrium probes, demonstrating an advantage despite their nonoptimality. It is possible to repeat the thermometric protocol on the prethermal state numerous times within the extended period that the system requires to achieve full thermalization. Repeated measurements lead to a statistical reduction in fluctuations of the temperature estimation, even when the protocol is not finely tuned for maximizing sensitivity.

Quantum probes exhibiting prethermal states can be engineered in Hamiltonians with nearly degenerate energy levels. In this study, we take the V model and its extension as a case study. The V model comprises three energy levels with a ground state and two nearly degenerate excited states. When weakly coupled to the bath, this system is known to exhibit a long-lived transient dynamics with the generation of coherences between excited levels [20,36–39]. This model is particularly relevant since it is an example of an optimal *equilibrium* thermal probe [11]. However, the long equilibration time that this system requires limits its practical utility. We analytically compute the quantum Fisher information of the V model and show that for a class of experimentally motivated initial conditions, the *optimal* protocol involves energy measurements of the *prethermal* probe. Even when using suboptimial protocols, the prethermal state allows for both high sensitivity and a dramatic reduction in the period required to perform the estimation protocol. This study thus opens the door to different architectures for quantum sensors where time as a resource is leveraged using prethermal probes.

Fundamental limits of quantum thermometry. The objective of thermometry is to acquire information about the temperature of the sample from measurements of the probe. To do this, one initially prepares the input state of the probe $\sigma(0)$ and allows it to interact with the sample, treated as a thermal reservoir, for a duration time t. During this interaction, the temperature information is encoded in the probe's state via $\sigma_\beta(t) = \mathcal{L}[\sigma(0)]$, where $\mathcal{L}$ denotes Markovian time evolution in the superoperator notation [40–42]. Information about the inverse temperature, the parameter β, is obtained by measuring a physical observable of the probe. The sensing precision is given by the Cramér-Rao bound [3,4],

$$\delta\beta \geqslant [M\mathcal{F}(\beta)]^{-1/2}, \tag{1}$$

where the uncertainty $[\delta\beta = (\langle\beta^2\rangle - \langle\beta\rangle^2)^{1/2}]$ is bounded from below by the inverse of the quantum Fisher information (QFI), the figure of merit for thermal sensitivity of each of the M independent measurements. The QFI is obtained from a maximization process over all measurement operators $\hat{O}$ of the classical Fisher information (CFI). It is useful to define it as $\mathcal{F}(\beta) = \mathrm{Tr}[\hat{L}_\beta^2\sigma_\beta(t)]$, where the symmetric logarithmic derivative $\hat{L}_\beta$ is given from $\partial_\beta\sigma_\beta(t) = \frac{1}{2}\{\hat{L}_\beta, \sigma_\beta(t)\}$ [1,5].

Prethermal thermometry. Prethermal states are stable, long-lived, transient states that the system populates before proceeding to its equilibrium state, enabling an *expedited* temperature estimation at the nanoscale. The key advantage of prethermal probes lies in saving the extended time required to prepare a thermal state within the probe. We do not need to optimize the measurement protocol to see an advantage; the time savings we get from estimating temperature using prethermal probes allows for many repetitions of the measurement protocol within the time interval necessary for a single equilibrium measurement. The outcome is the enhancement of the statistical factor M governing temperature precision, Eq. (1).

Prethermalization effects in unitary quantum systems have been discussed in many studies [33–35,43]. In open quantum systems, prethermal states develop when there is a large separation of timescales in the relaxation dynamics [44–46]. In particular, one needs to consider the eigenspectrum of the Liouvillian superoperator responsible for nonunitary dynamics [20]. For Markovian evolution, the state of the system can be expanded in terms of exponential functions with decay rates captured by the eigenvalues of the Liouvillian $\{\lambda_n\}$. The timescale to thermalize is dominated by the smallest-magnitude eigenvalue. Prethermal states exist when there is at least one eigenvalue (λ_1) that is much smaller in magnitude than the rest of the eigenvalues $(\lambda_{n>1})$, with the prethermal regime existing between the slowest and second-slowest active modes: $\tau_2 \leqslant t \leqslant \tau_1$; $\tau_n = 1/|\lambda_n|$ are the corresponding decay times.

Model. We consider the V model [36,38] as a case study for manifesting the advantage of prethermal thermometry over equilibrium thermometry. In this work, we set $\hbar \equiv 1$, and $k_B \equiv 1$. The Hamiltonian consists of the probe, the sample, and their coupling term, $\hat{H} = \hat{H}_S + \hat{S}\hat{B} + \hat{H}_B$. The probe includes three levels with two nearly degenerate excited states, $\hat{H}_S = (\nu - \Delta)\,|2\rangle\langle 2| + \nu\,|3\rangle\langle 3|$. The energy of the ground state is set to zero. The sample, described by $\hat{H}_B$, can be composed of any type of particles, even containing interactions between them. It is maintained in a thermal state at an inverse temperature β. The probe couples to the sample via $\hat{S} = |1\rangle\langle 2| + |1\rangle\langle 3| + \mathrm{H.c.}$ with $\hat{B}$ an operator of the sample. The probe-sample interaction is assumed weak thus noninvasive (contrasting Refs. [14,32,47]).

As demonstrated in Ref. [36], long-lived prethermal states develop when the excited states are nearly degenerate, $\nu \gg \Delta$, with Δ further being smaller than the thermal relaxation timescale k^{-1}.

We adopt the unified quantum master equation (UQME) approach, a simplified Redfield QME that preserves complete positivity and thermodynamic consistency of the quantum dynamics [48,49], and write down equations of motion for the average excited-state population $[p(t) = \frac{1}{2}[\sigma_{22}(t) + \sigma_{33}(t)]]$ and the real and imaginary parts of the coherences [20],

$$\begin{aligned}
\dot{p}(t) &= -k\sigma_{32}^R(t) - \phi p(t) + \frac{\phi - k}{2},\\
\dot{\sigma}_{32}^R(t) &= -k\sigma_{32}^R(t) - \phi p(t) + \Delta\sigma_{32}^I(t) + \frac{\phi - k}{2},\\
\dot{\sigma}_{32}^I(t) &= -k\sigma_{32}^I(t) - \Delta\sigma_{32}^R(t).
\end{aligned} \tag{2}$$

The Redfield QME builds on the Born-Markov approximation assuming weak (noninvasive) probe-sample coupling and fast dynamics in the sample [50]. The UQME further partially secularizes the dynamics, maintaining coherences only between states close in energy. The rate constant to transition from either of the excited states to the ground state is given by $k = \int_{-\infty}^{\infty} d\tau e^{i\nu\tau}\langle\hat{B}(\tau)\hat{B}(0)\rangle_B$. $\hat{B}(\tau)$ is given in the interaction picture and the thermal average is done with respect to the thermal state of the sample. The related rate $\phi \equiv k(1 + 2e^{-\beta\nu})$ is introduced for convenience. Results of

this study are given in terms of these rates, and are general for any type of sample and coupling operator $\hat{B}$. For concreteness, in simulations we assume samples comprising harmonic modes (phonons), $\hat{H}_B = \sum_j \omega_j \hat{b}_j^\dagger \hat{b}_j$, and coupled to the probe via $\hat{B} = \sum_j f_j(\hat{b}_j^\dagger + \hat{b}_j)$, with f_j the interaction energy to each mode. In this case, $k{=}2J(\nu)[n_B(\nu){+}1]$ with $J(\omega) = \pi \sum_j f_j^2 \delta(\omega - \omega_j)$ the spectral density of the sample.

We proceed to solve the unified QME (2) under the Liouvillian eigenvalue perturbation estimation (LEPE) technique of Ref. [20]. We organize the set of equations as $\frac{d\vec{v}}{dt} = L\vec{v}(t)$, with $\vec{v}(t) = [p(t), \sigma_{32}^R(t), \sigma_{32}^I(t)]^T$, and the Liouvillian constructed from Eq. (2). Following the LEPE procedure, keeping terms to the lowest order in Δ, the eigenvalues of the Liouvillian are given by $\lambda_1 \approx \frac{-\phi\Delta^2}{k(k+\phi)}$, $\lambda_2 \approx -k$, $\lambda_3 = -(\phi + k)$. Invoking an exponential ansatz for the Markovian dynamics, the solution of the equation of motion for a general initial condition for the population $p(0) = p_0$ and the real and imaginary coherences, $\sigma_{32}^R(0) = \sigma_0^R$, $\sigma_{32}^I(0) = \sigma_0^I$, is given by

$$\sigma_{32}^R(t) = \frac{1}{2(\phi+k)}\Big\{\big[\phi\big(1 + 2\sigma_0^R - 2p_0\big) - k\big]e^{-\frac{\phi\Delta^2}{k(k+\phi)}t} - \big[\phi(1-2p_0) - k\big(1 + 2\sigma_0^R\big)\big]e^{-(\phi+k)t}\Big\}, \tag{3}$$

$$p(t) = \frac{\phi - k}{2\phi} - \frac{1}{2(\phi+k)}\left\{\frac{k}{\phi}\big[\phi\big(1 + 2\sigma_0^R - 2p_0\big) - k\big]e^{-\frac{\phi\Delta^2}{k(k+\phi)}t} + \big[\phi(1-2p_0) - k\big(1 + 2\sigma_0^R\big)\big]e^{-(\phi+k)t}\right\}. \tag{4}$$

The imaginary part of the coherences is $\mathcal{O}(\Delta)$ and does not contribute significantly to the dynamics, thus to the Fisher information, as we also verify below with simulations. We highlight the appearance of two separate timescales in the dynamics as discussed in previous works, e.g., Refs. [20,36–39,51–53]: The short timescales $\tau_{2,3} = \lambda_{2,3}^{-1}$ dictate the time to reach prethermalization. The long timescale $\tau_1 = \lambda_1^{-1}$ is associated with full thermalization. The prethermal state (denoted by $\tilde{p}$ and $\tilde{\sigma}$) lives during the period $\tau_2 \leqslant t \leqslant \tau_1$. It can be approximated as constant (time independent) in this interval, reminiscent of a true equilibrium state, except with a dependence on the initial conditions, entirely captured by the parameter $\xi \equiv \sigma_0^R - p_0$,

$$\tilde{\sigma}_{32}^R = \frac{e^{-\beta\nu} + (1 + 2e^{-\beta\nu})\xi}{2(1 + e^{-\beta\nu})}, \quad \tilde{p} = \frac{e^{-\beta\nu} - \xi}{2(1 + e^{-\beta\nu})}. \tag{5}$$

For the density matrix to be physical, the initial conditions are constrained such that $-1 \leqslant \xi \leqslant 0$ [54].

In Fig. 1 we exemplify the dynamics of the V model with three different initial conditions: ground state preparation (blue), maximally mixed state (red), and an ambient (A) thermal state for the probe characterized by an inverse temperature $\beta_A \neq \beta$ (purple). We display the dynamics using the closed-form expressions (3) and (4). Results were benchmarked (not shown) against numerical results from the Born-Markov Redfield QME and we found a perfect agreement, as expected in the limit of small Δ. Figure 1 visualizes

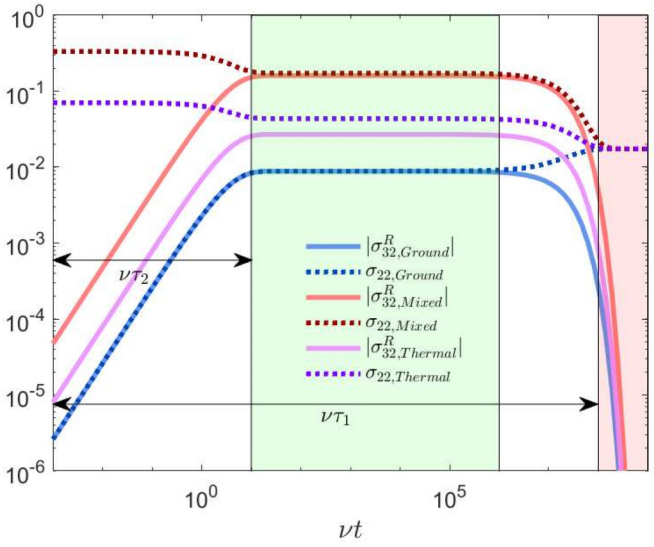

FIG. 1. The dynamics of coherences (solid) and excited-state populations (dotted) in the V model following Eqs. (3) and (4) displays two dynamical regimes: (i) Fast dynamics over τ_2, transitioning the initial condition to the prethermal state. (ii) Slow relaxation of the prethermal state extending the period $\tau_1 - \tau_2$ (shaded green region) towards thermal equilibrium (shaded red). The dynamics are studied for three initial conditions: (1) $p_0 = 0$ and $\sigma_0^{R,I} = 0$ (blue, "Ground"), (2) a maximally mixed state $p_0 = 1/3$, $\sigma_0^{R,I} = 0$ (red,"Mix") and (3) a thermal state at ambient temperature β_A with $p_0 = \frac{e^{-\beta_A\nu}}{1+2e^{-\beta_A\nu}}$ and $\sigma_0^{R,I} = 0$ (purple, "Thermal"). Parameters are $\nu = 1$, $\beta\nu = 4$, $\beta_A\nu = 2.5$, $\Delta = 10^{-4}\nu$. We adopt an Ohmic spectral density function, $J(\omega) = \gamma\omega$, with $\gamma = 0.07$.

the emergence of the two separate timescales, τ_2 and τ_1, associated with prethermalization and full thermalization, respectively. The prethermal state, captured by Eq. (5), relies on the buildup of quantum coherences between excited states (see also Refs. [20,36–38,51–53]). It is long lived, lasting for a time interval $(\tau_1 - \tau_2) \approx 10^6/\nu$. As such, it can serve as a robust alternative to thermal probes, bypassing long thermalization times. Figure 1 further exemplifies the dependence of prethermal states on initial conditions. The addition of decoherence will not affect the lifetime of the prethermal state, so long as the decoherence of excited states is correlated, which is expected for atomic or nanoscale probes.

We now compute the CFI and the QFI of a prethermal probe using Eq. (5) and show that for a class of experimentally motivated initial conditions, energy measurements are optimal, as in the equilibrium case. By definition, the CFI is given in terms of the populations p_j of the probe as $\mathcal{I}(\beta) = \sum_j \frac{1}{p_j}(\partial_\beta p_j)^2$ [1]. The CFI, which projects onto the eigenbasis of the Hamiltonian, extracts information from populations only. To obtain information from coherences as well, we need to compute the QFI, which by definition is given in terms of the symmetric logarithmic derivative, $\tilde{\mathcal{F}}(\beta) = \mathrm{Tr}[\hat{L}_\beta^2 \tilde{\sigma}_\beta]$. The prethermal state can easily be diagonalized [54]. Importantly, the transformation matrix is independent of temperature, which allows analytic computations of the symmetric logarithmic derivative from which the QFI can be computed. Substituting the prethermal state Eq. (5)

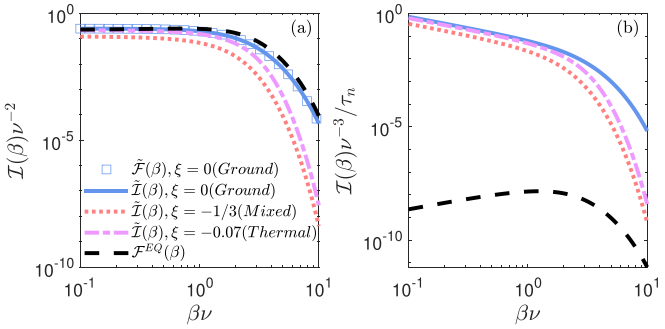

FIG. 2. Inverse temperature dependence of the equilibrium and prethermal (classical and quantum) Fisher information. We display the (a) Fisher information and (b) the time-weighted Fisher information, $\frac{1}{\tau_2}\tilde{\mathcal{I}}(\beta)$ for prethermal thermometry with ground state (blue), maximally mixed state (red), and ambient thermal state (purple) initialization as well as $\frac{1}{\tau_1}\mathcal{F}^{EQ}(\beta)$ for equilibrium thermometry (dashed). Parameters are the same as in Fig. 1.

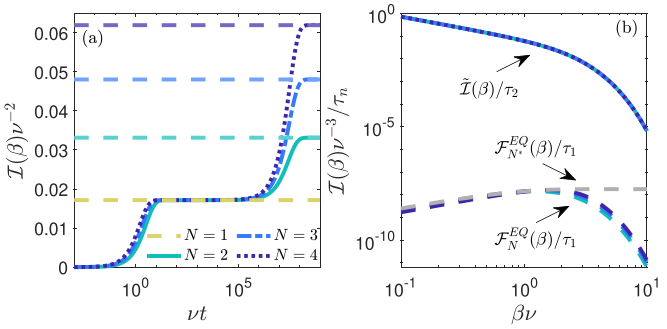

FIG. 3. N quasidegenerate-level prethermal probes with $N = 2, 3, 4$ excited states. (a) Time dependence of the QFI with a ground state initialization compared to the equilibrium QFI (constant dashed lines with N growing bottom to top). $N = 1$ corresponds to a qubit probe. (b) Corresponding time-weighted Fisher information as a function of inverse temperature. The gray dashed line is the equilibrium time-weighted Fisher information with N^* excited levels. We approximate $\tau_1 = \lambda_1^{-1}$ and $\tau_2 = \lambda_2^{-1}$ based on (a), assuming these times only mildly change with N for small N. Other parameters are the same as in Fig. 1.

into the definition of the CFI and the QFI, we get, respectively,

$$\tilde{\mathcal{I}}(\beta) = \frac{\nu^2 e^{\nu\beta}[\xi + 1]}{(1 + e^{\nu\beta})^2(1 - \xi e^{\nu\beta})}, \tag{6}$$

and

$$\tilde{\mathcal{F}}(\beta) = \frac{\nu^2 e^{\nu\beta}[\xi + 1]}{(1 + e^{\nu\beta})^2}. \tag{7}$$

In the special case where $\xi = 0$, e.g., a ground state initialization, the QFI reduces to the CFI. The interpretation of this correspondence is that in this case, coherences add no further information about temperature than the populations already bring. We further note that the QFI is strictly greater than or equal to the CFI, as required, since $\xi \leqslant 0$ [54]. Optimal QFI and CFI arise when $\xi = 0$, with the initial and prethermal populations and coherences being equal, resulting in the highest thermal sensitivity of energy measurements. We contrast the prethermal values of the QFI and CFI with the QFI obtained at equilibrium, where energy measurements are optimal, given by

$$\mathcal{F}^{\mathrm{EQ}}(\beta) = \frac{2\nu^2 e^{\nu\beta}}{(2 + e^{\nu\beta})^2}. \tag{8}$$

Comparing this result to Eq. (7), we conclude that the prethermal probe provides similar precision as the equilibrium one for a single measurement at high temperatures [see also Fig. 2(a)]. However, the *time* required for temperature estimation is substantial in the equilibrium case, given the long thermalization time. Therefore, the relevant figure of merit is the Fisher information *divided by the time it takes to prepare the state over which temperature estimation is performed*. This time-weighted quantum Fisher information (TQFI) is given by $\frac{1}{\tau_2}\tilde{\mathcal{F}}(\beta)$ for prethermal thermometry and $\frac{1}{\tau_1}\mathcal{F}^{\mathrm{EQ}}(\beta)$ for equilibrium thermometry. Corresponding definitions hold for the time-weighted classical Fisher information (TCFI).

We contrast the prethermal CFI and QFI with the equilibrium QFI in Fig. 2(a). The equilibrium QFI (black dashed) is roughly equal to a prethermal QFI with a ground state preparation (blue squares), which also *equals* the CFI (blue solid line). This indicates that energy measurements remain optimal during prethermalization for ground state preparations. We observe though the loss of sensitivity of energy measurements at low temperature when the V model is initialized as a maximally mixed state (red) or as an ambient thermal state (purple). However, as mentioned above, the relevant figure of merit for thermometry should take into account the time it takes to arrive at the state used for metrology. Using the TCFI, Fig. 2(b) demonstrates an *orders of magnitude* advantage in sensitivity for prethermal probes over the corresponding equilibrated probes. Most notably, despite energy measurements being suboptimal for non-ground-state preparations, significant time is saved in state preparation. This time can be used to perform more measurements, offering a great reduction in statistical fluctuations through the factor M in Eq. (1). Namely, for the same period, the ratio between the number of measurements when using prethermal probes ($\tilde{M}$) to that number with equilibrated probes (M^{EQ}) is $\tilde{M}/M^{\mathrm{EQ}} \approx \tau_1/\tau_2$, translating to an improvement of $\sqrt{\tau_1/\tau_2}$ in precision. Based on Fig. 1, $\tau_1/\tau_2 \approx 10^6$, thus we achieve a factor of 1000 improvement in thermal sensitivity when using prethermal probes, compared to the equilibrium protocol.

N-level probes. So far, we exemplified the advantage of prethermal thermometry using the V model as a case study. However, our results are more general and robust. We consider the optimal equilibrium probe suggested in Ref. [11], with N nearly degenerate excited states and a single ground state. We obtain the equilibrium QFI [54]

$$\mathcal{F}^{\mathrm{EQ}}_N(\beta) = \frac{N\nu^2 e^{\nu\beta}}{(N + e^{\nu\beta})^2}. \tag{9}$$

Notably, this QFI is maximized at $N^* = e^{\beta\nu}$ with $\mathcal{F}^{\mathrm{EQ}}_{N^*}(\beta) = \nu^2/4$. Simulating the Redfield QME, we demonstrate in Fig. 3(a) the time dependence of the QFI for an initial ground state preparation for $N = 2$ (teal), $N = 3$ (blue), and $N = 4$

(purple) excited levels. We find that the long-lived prethermal state is robust, and approximately constant with N. The equilibrium QFI grows with N in this regime, while the prethermal QFI is constant. We further display (gold) the qubit ($N = 1$) equilibrium QFI in Fig. 3(a) showing that the equilibrium qubit probe performs equally well to the prethermal probes. We discuss this agreement further in the Supplemental Material [54]. Note that a qubit probe does not display a long-lived transient dynamics. Using the proper measure, which is the TCFI, in Fig. 3(b), we find that $\tilde{\mathcal{I}}(\beta)/\tau_2$ is about five orders of magnitude greater than the equilibrium value Eq. (9), even when using the most optimal equilibrium setup, $\mathcal{F}^{\mathrm{EQ}}_{N^*}(\beta)/\tau_1$ (gray). Note that when $\beta\nu \gtrsim 4$, $N^* > 50$, which is impractical. This establishes that optimal equilibrium thermometers cannot reach the level of precision of transient thermometry when compared with the proper TQFI/TCFI measure.

Conclusions. Systems with a series of degenerate excited states are optimized for sensitivity for equilibrium thermometry, yet they require extremely long times to reach thermal equilibrium due to the development of quantum coherences between degenerate levels. Instead, we introduced here the concept of prethermal thermometry, where long-lived quasistationary states were utilized as robust thermometers. The dramatic advantage of prethermal probes over their equilibrium counterparts arises from saving extreme long contact times required to reach thermal equilibrium in such setups. Considering the V model as a case study, we calculated analytically the QFI and CFI for prethermal probes and demonstrated orders-of-magnitude improvement in the time-weighted figure of merit for precision. Generalization to N-excited levels demonstrated that the advantage of prethermal thermometry is significant even when compared to an optimized equilibrium probe. Depending on the temperature range, experimental realizations could build on atomic [55], vibrational [56], or rotational levels and other engineered or naturally occurring spin impurities [57,58]. Moreover, prethermal thermometry could be leveraged with newly developed Bayesian tools [59–62]. Altogether, prethermal thermometry drawing upon quantum coherences and other mechanisms offers a different pathway for achieving accurate, robust, and rapid temperature estimation at the nanoscale, particularly suited for weakly coupled, minimally invasive scenarios.

Acknowledgments. D.S. acknowledges support from an NSERC Discovery Grant and the Canada Research Chair program. The work of N.A.S. was supported by Ontario Graduate Scholarship (OGS) and an Alliance Catalyst Quantum Grant. H.J.D.M. acknowledges funding from a Royal Society Research Fellowship (URF/R1/231394), and the Royal Commission for the Exhibition of 1851.

[1] M. Mehboudi, A. Sanpera, and L. A. Correa, Thermometry in the quantum regime: Recent theoretical progress, J. Phys. A: Math. Theor. **52**, 303001 (2019).

[2] *Thermodynamics in the Quantum Regime: Fundamental Aspects and New Directions*, edited by F. Binder, L. A. Correa, C. Gogolin, J. Anders, and G. Adesso, Fundamental Theories of Physics (Springer, Cham, 2018), Vol. 195, pp. 1–2.

[3] C. L. Degen, F. Reinhard, and P. Cappellaro, Quantum sensing, Rev. Mod. Phys. **89**, 035002 (2017).

[4] V. Giovanetti, S. Lloyd, and L. Maccone, Advances in quantum metrology, Nat. Photon. **5**, 222 (2011).

[5] J. Liu, J. Chen, X.-X. Jing, and X. Wang, Quantum Fisher information and symmetric logarithmic derivative via anticommutators, J. Phys. A: Math. Theor. **49**, 275302 (2016).

[6] *Thermometry at the Nanoscale: Techniques and Selected Applications*, edited by L. D. Carlos and F. Palacio (The Royal Society of Chemistry, London, 2015).

[7] G. W. Walker, V. C. Sundar, C. M. Rudzinski, A. W. Wun, M. G. Bawendi, and D. G. Nocera, Quantum-dot optical temperature probes, Appl. Phys. Lett. **83**, 3555 (2003).

[8] C. T. Nguyen, R. E. Evans, A. Sipahigil, M. K. Bhaskar, D. D. Sukachev, V. N. Agafonov, V. A. Davydov, L. F. Kulikova, F. Jelezko, and M. D. Lukin, All-optical nanoscale thermometry with silicon-vacancy centers in diamond, Appl. Phys. Lett. **112**, 203102 (2018).

[9] Q. Bouton, J. Nettersheim, D. Adam, F. Schmidt, D. Mayer, T. Lausch, E. Tiemann, and A. Widera, Single-atom quantum probes for ultracold gases boosted by nonequilibrium spin dynamics, Phys. Rev. X **10**, 011018 (2020).

[10] J. Glatthard, K. V. Hovhannisyan, M. Perarnau-Llobet, L. A. Correa, and H. J. D. Miller, Energy measurements remain thermometrically optimal beyond weak coupling, Quantum **7**, 1190 (2023).

[11] L. A. Correa, M. Mehboudi, G. Adesso, and A. Sanpera, Individual quantum probes for optimal thermometry, Phys. Rev. Lett. **114**, 220405 (2015).

[12] P. Abiuso, P. Andrea Erdman, M. Ronen, F. Noé, G. Haack, and M. Perarnau-Llobet, Optimal thermometers with spin networks, Quantum Sci. Technol. **9**, 035008 (2024).

[13] S. Campbell, M. G. Genoni, and S. Deffner, Precision thermometry and the quantum speed limit, Quantum Sci. Technol. **3**, 025002 (2018).

[14] L. A. Correa, M. Perarnau-Llobet, K. V. Hovhannisyan, S. Hernández-Santana, M. Mehboudi, and A. Sanpera, Enhancement of low-temperature thermometry by strong coupling, Phys. Rev. A **96**, 062103 (2017).

[15] S. Seah, S. Nimmrichter, D. Grimmer, J. P. Santos, V. Scarani, and G. T. Landi, Collisional quantum thermometry, Phys. Rev. Lett. **123**, 180602 (2019).

[16] C. L. Latune, I. Sinayskiy, and F. Petruccione, Collective heat capacity for quantum thermometry and quantum engine enhancements, New J. Phys. **22**, 083049 (2020).

[17] M. Płodzień, R. Demkowicz-Dobrzański, and T. Sowiński, Few-fermion thermometry, Phys. Rev. A **97**, 063619 (2018).

[18] S. Campbell, M. Mehboudi, G. D. Chiara, and M. Paternostro, Global and local thermometry schemes in coupled quantum systems, New J. Phys. **19**, 103003 (2017).

[19] A. Ullah, M. T. Naseem, and Ö. E. Müstecaplıoğlu, Low-temperature quantum thermometry boosted by coherence generation, Phys. Rev. Res. **5**, 043184 (2023).

[20] F. Ivander, N. Anto-Sztrikacs, and D. Segal, Hyperacceleration of quantum thermalization dynamics by bypassing long-lived coherences: An analytical treatment, Phys. Rev. E **108**, 014130 (2023).

[21] S. Dooley, W. J. Munro, and K. Nemoto, Quantum metrology including state preparation and readout times, Phys. Rev. A **94**, 052320 (2016).

[22] A. J. Hayes, S. Dooley, W. J. Munro, K. Nemoto, and J. Dunningham, Making the most of time in quantum metrology: concurrent state preparation and sensing, Quantum Sci. Technol. **3**, 035007 (2018).

[23] M. T. Mitchison, T. Fogarty, G. Guarnieri, S. Campbell, T. Busch, and J. Goold, *In situ* thermometry of a cold Fermi gas via dephasing impurities, Phys. Rev. Lett. **125**, 080402 (2020).

[24] M. T. Mitchison, A. Purkayastha, M. Brenes, A. Silva, and J. Goold, Taking the temperature of a pure quantum state, Phys. Rev. A **105**, L030201 (2022).

[25] S. Brattegard and M. T. Mitchison, Thermometry by correlated dephasing of impurities in a 1D Fermi gas, Phys. Rev. A **109**, 023309 (2024).

[26] S. Jevtic, D. Newman, T. Rudolph, and T. M. Stace, Single-qubit thermometry, Phys. Rev. A **91**, 012331 (2015).

[27] V. Cavina, L. Mancino, A. De Pasquale, I. Gianani, M. Sbroscia, R. I. Booth, E. Roccia, R. Raimondi, V. Giovannetti, and M. Barbieri, Bridging thermodynamics and metrology in nonequilibrium quantum thermometry, Phys. Rev. A **98**, 050101(R) (2018).

[28] M. M. Feyles, L. Mancino, M. Sbroscia, I. Gianani, and M. Barbieri, Dynamical role of quantum signatures in quantum thermometry, Phys. Rev. A **99**, 062114 (2019).

[29] L. Mancino, M. G. Genoni, M. Barbieri, and M. Paternostro, Nonequilibrium readiness and precision of Gaussian quantum thermometers, Phys. Rev. Res. **2**, 033498 (2020).

[30] A. H. Kiilerich, A. De Pasquale, and V. Giovannetti, Dynamical approach to ancilla-assisted quantum thermometry, Phys. Rev. A **98**, 042124 (2018).

[31] P. Sekatski and M. Perarnau-Llobet, Optimal nonequilibrium thermometry in Markovian environments, Quantum **6**, 869 (2022).

[32] Z.-Z. Zhang and W. Wu, Non-Markovian temperature sensing, Phys. Rev. Res. **3**, 043039 (2021).

[33] M. Ueda, Quantum equilibration, thermalization and prethermalization in ultracold atoms, Nat. Rev. Phys. **2**, 669 (2020).

[34] K. Mallayya, M. Rigol, and W. De Roeck, Prethermalization and thermalization in isolated quantum systems, Phys. Rev. X **9**, 021027 (2019).

[35] M. Gring, M. Kuhnert, T. Langen, T. Kitagawa, B. Rauer, M. Schreitl, I. Mazets, D. A. Smith, E. Demler, and J. Schmiedmayer, Relaxation and prethermalization in an isolated quantum system, Science **337**, 1318 (2012).

[36] T. V. Tscherbul and P. Brumer, Long-lived quasistationary coherences in a V-type system driven by incoherent light, Phys. Rev. Lett. **113**, 113601 (2014).

[37] T. V. Tscherbul and P. Brumer, Partial secular Bloch-Redfield master equation for incoherent excitation of multilevel quantum systems, J. Chem. Phys. **142**, 104107 (2015).

[38] A. Dodin, T. V. Tscherbul, and P. Brumer, Coherent dynamics of V-type systems driven by time-dependent incoherent radiation, J. Chem. Phys. **145**, 244313 (2016).

[39] M. Merkli, H. Song, and G. P. Berman, Multiscale dynamics of open three-level quantum systems with two quasi-degenerate levels, J. Phys. A: Math. Theor. **48**, 275304 (2015).

[40] H. P. Breuer and F. Petruccione, *The Theory of Open Quantum Systems* (Oxford University Press, New York, 2002).

[41] U. Weiss, *Quantum Dissipative Systems* (World Scientific, Singapore, 1999).

[42] R. Hartmann and W. T. Strunz, Accuracy assessment of perturbative master equations: Embracing nonpositivity, Phys. Rev. A **101**, 012103 (2020).

[43] T. Mori, T. N. Ikeda, E. Kaminishi, and M. Ueda, Thermalization and prethermalization in isolated quantum systems: a theoretical overview, J. Phys. B: At., Mol. Opt. Phys. **51**, 112001 (2018).

[44] A. Anglés-Castillo, M. C. Bañuls, A. Pérez, and I. D. Vega, Prethermalization of quantum systems interacting with non-equilibrium environments, New J. Phys. **22**, 083067 (2020).

[45] K. Macieszczak, D. C. Rose, I. Lesanovsky, and J. P. Garrahan, Theory of classical metastability in open quantum systems, Phys. Rev. Res. **3**, 033047 (2021).

[46] K. Macieszczak, M. Guţă, I. Lesanovsky, and J. P. Garrahan, Towards a theory of metastability in open quantum dynamics, Phys. Rev. Lett. **116**, 240404 (2016).

[47] M. Brenes and D. Segal, Multispin probes for thermometry in the strong-coupling regime, Phys. Rev. A **108**, 032220 (2023).

[48] A. Trushechkin, Unified Gorini-Kossakowski-Lindblad-Sudarshan quantum master equation beyond the secular approximation, Phys. Rev. A **103**, 062226 (2021).

[49] M. Gerry and D. Segal, Full counting statistics and coherences: Fluctuation symmetry in heat transport with the unified quantum master equation, Phys. Rev. E **107**, 054115 (2023).

[50] A. Nitzan, *Chemical Dynamics in Condensed Phases: Relaxation, Transfer, and Reactions in Condensed Molecular Systems* (Oxford University Press, New York, 2006).

[51] A. Dodin, T. V. Tscherbul, and P. Brumer, Quantum dynamics of incoherently driven V-type systems: Analytic solutions beyond the secular approximation, J. Chem. Phys. **144**, 244108 (2016).

[52] A. Dodin and P. Brumer, Noise-induced coherence in molecular processes, J. Phys. B: At., Mol. Opt. Phys. **54**, 223001 (2022).

[53] F. Ivander, N. Anto-Sztrikacs, and D. Segal, Quantum coherence-control of thermal energy transport: the V model as a case study, New J. Phys. **24**, 103010 (2022).

[54] See Supplemental Material at http://link.aps.org/supplemental/10.1103/PhysRevA.109.L060201 for (S1) details on the calculation of the quantum Fisher information and the classical Fisher information for the V model using prethermal and thermal probes, (S2) comparison of results to a qubit probe, (S3) discussion over valid initial conditions for the V model, and (S4) derivation of the quantum Fisher information for an N-degenerate level thermal probe.

[55] A. Dodin, T. Tscherbul, R. Alicki, A. Vutha, and P. Brumer, Secular versus nonsecular Redfield dynamics and Fano coherences in incoherent excitation: An experimental proposal, Phys. Rev. A **97**, 013421 (2018).

[56] N. B. Vilas, C. Hallas, L. Anderegg, P. Robichaud, C. Zhang, S. Dawley, L. Cheng, and J. M. Doyle, Blackbody

thermalization and vibrational lifetimes of trapped polyatomic molecules, Phys. Rev. A **107**, 062802 (2023).

[57] E. Bauch, S. Singh, J. Lee, C. A. Hart, J. M. Schloss, M. J. Turner, J. F. Barry, L. M. Pham, N. Bar-Gill, S. F. Yelin, and R. L. Walsworth, Decoherence of ensembles of nitrogen-vacancy centers in diamond, Phys. Rev. B **102**, 134210 (2020).

[58] S. Hernández-Gómez, S. Gherardini, N. Staudenmaier, F. Poggiali, M. Campisi, A. Trombettoni, F. S. Cataliotti, P. Cappellaro, and N. Fabbri, Autonomous dissipative Maxwell's demon in a diamond spin qutrit, PRX Quantum **3**, 020329 (2022).

[59] J. Rubio, J. Anders, and L. A. Correa, Global quantum thermometry, Phys. Rev. Lett. **127**, 190402 (2021).

[60] J. Glatthard, J. Rubio, R. Sawant, T. Hewitt, G. Barontini, and L. A. Correa, Optimal cold atom thermometry using adaptive bayesian strategies, PRX Quantum **3**, 040330 (2022).

[61] M. Mehboudi, M. R. Jørgensen, S. Seah, J. B. Brask, J. Kołodyński, and M. Perarnau-Llobet, Fundamental limits in Bayesian thermometry and attainability via adaptive strategies, Phys. Rev. Lett. **128**, 130502 (2022).

[62] G. O. Alves and G. T. Landi, Bayesian estimation for collisional thermometry, Phys. Rev. A **105**, 012212 (2022).